RESEARCH ARTICLE | JUNE 10 2025

Challenges in modulation doping of n-type Ge/SiGe heterostructures: The role of epitaxial and thermal strain

E. Campagna ; E. Talamas Simola ; L. Di Gaspare ; D. Marian ; M. H. Zoellner ; F. Berkmann ; L. Baldassarre ; M. Ortolani ; G. Capellini ; M. Virgilio ; M. De Seta

APL Mater. 13, 061112 (2025)
https://doi.org/10.1063/5.0259848

Challenges in modulation doping of n-type Ge/SiGe heterostructures: The role of epitaxial and thermal strain

Cite as: APL Mater. 13, 061112 (2025); doi: 10.1063/5.0259848
Submitted: 21 January 2025 • Accepted: 24 May 2025 •
Published Online: 10 June 2025

E. Campagna,[1] E. Talamas Simola,[1] L. Di Gaspare,[1] D. Marian,[2] M. H. Zoellner,[3] F. Berkmann,[4] L. Baldassarre,[5] M. Ortolani,[5] G. Capellini,[1,3] M. Virgilio,[2,a)] and M. De Seta[1,b)]

AFFILIATIONS

[1] Dipartimento di Scienze, Università degli Studi Roma Tre, Viale G. Marconi 446, Roma 00146, Italy
[2] Dipartimento di Fisica "E. Fermi," Università di Pisa, Largo Pontecorvo 3, Pisa 56127, Italy
[3] IHP-Leibniz Institut für Innovative Mikroelektronik, Im Technologiepark 25, Frankfurt (Oder) 15236, Germany
[4] EFM—Experimental Physics and Functional Materials, BTU Cottbus, 03046 Cottbus, Germany
[5] Department of Physics, Sapienza Università di Roma, Piazzale Aldo Moro 2, 00185 Rome, Italy

[a)] **Author to whom correspondence should be addressed:** michele.virgilio@unipi.it
[b)] **Electronic mail:** monica.deseta@uniroma3.it

ABSTRACT

N-type Ge-rich Ge/SiGe multi-quantum-wells on Si(001) substrates are a novel material system with great potential due to their compatibility with the CMOS standard. This class of strained quantum heterostructures exhibits different band edge minima in a narrow energy range. Thus, lattice deformation, quantum confinement, and band bending effects can affect the energy ordering of the associated subband states, resulting in a radical variation of their optical and transport properties. This study investigates how these factors influence the 2D subband carrier density in modulation-doped heterostructures. To this end, we focus on the recently demonstrated parabolic quantum well system because of its technological relevance. Using Fourier transform infrared and high-resolution x-ray diffraction spectroscopy in combination with numerical modeling, our results highlight the importance of the temperature dependence of the strain field in determining the efficiency of the charge transfer process. Furthermore, optimal design parameters are identified to achieve either the highest transfer efficiency or the absolute value of the carrier density as a function of the intersubband transition energy in the 3–8 THz range.

N-type Ge-rich SiGe multilayer heterostructures have great potential due to their compatibility with CMOS technology.[1–3] However, the realization of frontier optoelectronic devices based on this material system has been demonstrated only recently, due to peculiar challenges that have hindered the development of Ge-rich group IV epitaxy.[1,4,5] Indeed, sharp or continuously graded heterointerfaces with highly reproducible chemical profiles extending over several microns have been demonstrated on Si substrates in the last few years only.[4–7] The achieved high crystal quality[8] of these complex planar heterostructures requires mastering the epitaxial strain field $\varepsilon_{\parallel}^{epi}$, associated with the large lattice mismatch existing between silicon (a_{Si} = 5.431 Å) and germanium (a_{Ge} = 5.658 Å). This is typically addressed by using a $Si_{1-y}Ge_y$ virtual substrate (VS) whose lattice parameter, controlled by the y Ge molar fraction, is chosen to reciprocally compensate the tensile and compressive biaxial lattice deformation of the different layers composing the heterostructure, a condition that promotes the mechanical stability during the epitaxial growth of thick multilayers. As an example, for a heterostructure comprising the periodic repetition of a $Si_{1-x}Ge_x$ barrier and a Ge well layer having equal thicknesses, the y concentration of a fully relaxed VS has to be set exactly half way between x and 1 to compensate for the tensile deformation occurring in the barrier layers with the compressive one featured by the Ge wells.

In addition to the presence of this epitaxial strain, it must be considered that, upon cooling the heterostructures from the growth

temperature (typically in the 650–800 K range), the strain field in each layer is also affected by the thermal strain in the plane $\varepsilon_{\parallel}^{therm}$ arising from the mismatch of the thermal expansion coefficient $\alpha(T)$ existing between the Si substrate and the Ge-rich active region. Therefore, the total in-plane strain experienced by each layer can be expressed as $\varepsilon_{\parallel} = \varepsilon_{\parallel}^{epi} + \varepsilon_{\parallel}^{therm}$.

The strain field has a direct impact on the electronic structure. As such, it has been used to engineer transport and optical properties, for example, in transistors[9] or in light emitters.[10] Furthermore, by modifying the band offsets at the heterointerfaces, the lattice strain can have an impact on vertical tunneling transport[3,4,11] and influence the charge transfer mechanism in modulation-doped heterostructures.[12] Accurate strain management is, therefore, critical, especially at low temperatures where the total strain is significantly enhanced by the increased contribution of the in-plane thermal strain component $\varepsilon_{\parallel}^{therm}$ (see Ref. 8). This is essential for optimizing the design and performance of SiGe-based quantum devices, including quantum cascade lasers, resonant tunneling diodes, and optical detectors and modulators that exploit light–matter interaction in the strong coupling regime. In this latter case, the achievement of the strong coupling condition requires carrier sheet densities exceeding 2×10^{11} cm^{-2}, underscoring the need for efficient and well-controlled transfer doping strategies.[5]

We recall here that Ge-rich $Si_{1-x}Ge_x$ alloys feature different band edges in a narrow energy interval above the absolute conduction minimum. In Ge, this minimum is located at the fourfold degenerate L point of the BZ, while for Ge content $x \lesssim 0.82$, it lies at the bottom of the sixfold degenerate Δ valleys. The strain field influences the energy separation of the L and Δ states since both react to the hydrostatic component of the lattice distortion; furthermore, the uniaxial part splits the energy of the Δ_6 states into Δ_4 and Δ_2 separate levels, pushing toward lower (higher) energies the Δ_2 valleys with respect to the Δ_4 ones when an in-plane tensile (compressive) biaxial deformation is applied. In light of the above considerations and due to the modest values of the conduction band offset at L featured by the Ge-rich SiGe/Ge heterointerface, a barrier Ge concentration x around 0.80 represents a typical trade-off to guarantee an effective confinement potential ΔE_{L-L} for the L carriers (of the order of 130 meV) and enough energy separation $\Delta E_{\Delta-L}$ between the absolute conduction band minima in the SiGe barrier (at Δ_2) and in the Ge well (at L).[12]

The relative energy separation of the Δ_2 and L subband states, respectively confined in the barrier and well regions, is key in determining both the transport and the optical properties of a given heterostructure. Such energy difference strongly depends on the chemical profile, lattice strain, confinement masses, and band bending effects, and a modification of its value significantly affects the efficiency of the well charging mechanisms, as in modulation-doped heterostructures the donor states are associated with the barrier Δ_2 levels.

To shed light on this last point, in this work we investigate the impact of epitaxial and thermal strain, confinement energy, and band bending effects on the transfer charge process in modulation-doped n-type Ge/SiGe quantum structures. To this aim, we focus on the recently demonstrated Ge/SiGe parabolic quantum wells (PQWs) because of their relevance for photonic applications in the THz range,[5,7,13–16] which is associated with the stability of their optical properties against temperature variations. As a matter of fact, modulation-doped PQWs feature a single intersubband transition (ISBT) absorption resonance, whose energy is largely independent of the carrier density and distribution in the subbands.[17] This characteristic makes PQWs an ideal quantum system for assessing the amount of transferred charge in the well by measuring the ISBT spectral weight.[18,19]

We combined high-resolution x-ray diffraction (HR-XRD) and Fourier transform infrared (FTIR) spectroscopy measurements on state-of-the-art *n*-type compositional graded Ge/SiGe PQWs grown by ultrahigh-vacuum chemical vapor deposition (UHV-CVD) on silicon substrates,[5,7,19] together with electronic states modeling based on a multi-valley Schroedinger–Poisson solver,[12] to provide valuable insight for design optimization, with a focus on precisely controlling the quantum well charging process, as required for various applications.[5,16]

The investigated samples consist of a periodic stack of Ge-rich PQWs separated by $Si_{0.18}Ge_{0.82}$ barriers having a thickness b = 15 nm. The multilayer structures, sketched in Fig. 1(a), have been grown on Si after the deposition of a reverse graded almost fully relaxed $Si_{1-y}Ge_y$ VS, whose final y value was varied in the range y = 0.85–0.91 to strain-balance the QW region and prevent its plastic relaxation.[8] The growth temperature of both the VS and the multilayer stack was T_G = 753 K. The parabolic confining potential was realized by continuously varying the Ge content in the region between two $Si_{0.18}Ge_{0.82}$ barrier layers up to 100%, which corresponds to the bottom of the PQWs. The compositional Ge content profile, measured by means of scanning transmission electron microscopy (STEM) and secondary ion mass spectrometry (SIMS), is shown in Fig. 1(b) for one of the investigated samples (S1), indicating a highly reproducible match with the nominal compositional profile. To shed light on the corresponding confining potential, we show in the inset of Fig. 1(a) the band-edge values at a $Si_{0.18}Ge_{0.82}$/Ge heterojunction, lattice matched to a cubic VS with y = 0.9, which represents the discontinuities occurring between the barrier and the bottom of the PQW.

Doping was achieved by phosphorus co-deposition in the d = 8–10 nm thick central region of the barrier. The donor concentration N_P has been tuned around 10^{18} cm^{-3} to obtain a total 2D carrier density per period, available for the transfer doping process, of $n_{2D}^{tot} = N_P \times d$ in the $[1–15] \times 10^{11}$ cm^{-2} range, as typically used in quantum devices. The SIMS profiles for the donor atoms in PQW samples are in good agreement with the nominal profiles, demonstrating that the P ions remain well confined in the barrier region (see Ref. 19). The comparison of the donor density measured by SIMS on thick test samples with the activated electron density obtained by optical reflectivity and Hall effect measurements indicates a donor activation ratio of ~100%, suggesting the absence of dopant segregation effects for impurity density at the 10^{18} cm^{-3} scale. Finally, the SIMS analysis highlights the presence of an exponential dopant diffusion tail with a characteristic length scale of only 3.5 nm.

Figure 1(a) evidences that the conduction band minimum occurs at L in the Ge compressive strained well and at Δ_2 in the tensile strained $Si_{0.18}Ge_{0.82}$ barrier. In this condition, we calculate a band offset ΔE_{L-L} at the L point of about 112 meV. The energy difference $\Delta E_{\Delta-L}$ is relatively small, around 50 meV. A reversed Δ_2 alignment

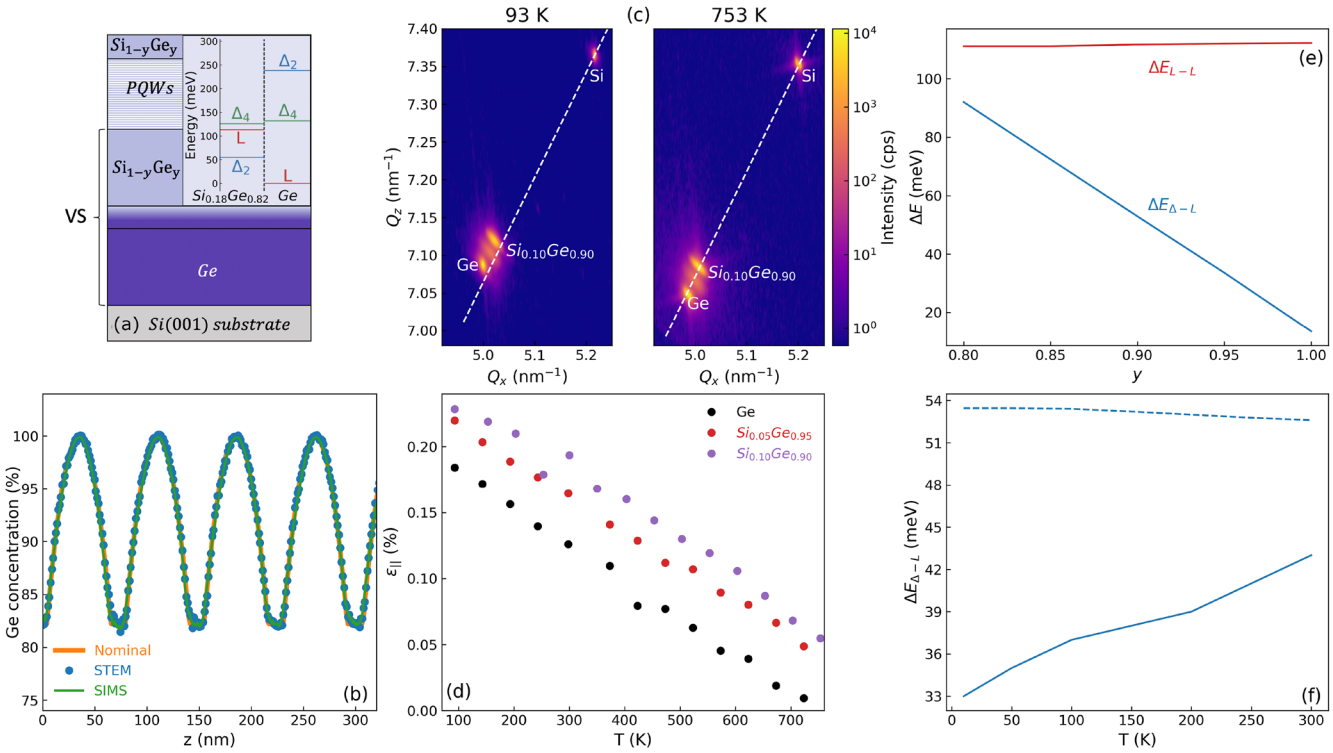

FIG. 1. (a) Sketch of the deposited multilayer structure. The periodic stack composed of PQWs and the $Si_{0.18}Ge_{0.82}$ barriers is deposited on top of the reverse graded relaxed $Si_{1-y}Ge_y$ VS. The inset shows the calculated energy positions of L, Δ_2, and Δ_4 band edges at a $Si_{0.18}Ge_{0.82}$/Ge heterointerface for $y = 0.9$. (b) Nominal Ge compositional profile for the PQW S1 sample along the growth direction (orange), compared with the ones measured by means of STEM (blue) and by SIMS (green). (c) (224) XRD maps of a reverse graded VS with final Ge content $y = 0.9$, acquired at 93 and 753 K. The dashed white line represents the calculated component of the transferred momentum for a relaxed cubic SiGe alloy. (d) In-plane strain $\varepsilon_\parallel(T)$ of the Ge and $Si_{0.1}Ge_{0.9}$ layers of the VS as a function of the temperature resulting from the XRD measurements. The data relative to a $Si_{0.05}Ge_{0.95}$ VS are also shown for comparison. (e) Calculated energy differences between the Δ_2–L and L–L edges at the $Si_{0.18}Ge_{0.82}$/Ge heterointerface at low T as a function of the VS Ge content y. (f) Calculated $\Delta E_{\Delta-L}$ as a function of T, including (continuous line) and neglecting (dashed line) the thermal strain for the same interface of (d) with $y = 0.9$.

is observed, leading to Δ_2 subband confinement within the SiGe barrier layers. It is important to note that the strain-dependent values of ΔE_{L-L} and $\Delta E_{\Delta-L}$ play a critical role in determining carrier confinement within the Ge well and the effectiveness of the transfer doping mechanism, respectively.

To disentangle the thermal and epitaxial contribution to the lattice strain field, we have first experimentally quantified $\varepsilon_\parallel(T)$ in two SiGe reversed graded VS samples featuring a final Ge concentration $y = 0.9$ and $y = 0.95$, using high resolution (224) XRD maps acquired in the temperature range spanning between 93 K and the growth temperature $T_G = 753$ K.

In Fig. 1(c), we display the XRD reciprocal space maps acquired on the $Si_{0.1}Ge_{0.9}$ VS at $T_G = 93$ K (left) and $T = 753$ K (right). The white dashed line represents the so-called "relaxation line" that evidences the relationship between the in-plane component Q_x and the out-of-plane component Q_z of the momentum transfer vector for a relaxed (cubic) lattice cell. We can clearly distinguish at $Q_x \simeq 5.2$ nm^{-1} the (224) peak of the Si reciprocal lattice point (RLP) corresponding to the substrate lattice, which moves along the relaxation line as the temperature changes, maintaining its cubic symmetry. At a lower value of $Q_x \simeq 5.0$ nm^{-1}, we observe the RLPs corresponding to the virtual substrate, with the two most intense peaks associated with the constant composition Ge and $Si_{0.1}Ge_{0.9}$ layer. It is evident that upon lowering T, the RLPs of Ge and $Si_{0.1}Ge_{0.9}$ layers move above the relaxation line, pointing to an accumulation of in-plane tensile strain in the VS.[20]

From XRD maps, the temperature dependence of $\varepsilon_\parallel$ in the SiGe and Ge layers can be quantitatively assessed in the whole temperature range of interest, following Ref. 20. As shown in Fig. 1(d), the $Si_{0.1}Ge_{0.9}$ and Ge lattices are practically fully relaxed around the growth temperature, while the lowering of T induces a monotonic increase in the tensile biaxial strain, whose value at 73 K is of the order of 0.2%. The T-independent offset that appears between the $Si_{0.1}Ge_{0.9}$ and Ge $\varepsilon_\parallel(T)$ values in Fig. 1(d) is to be attributed to the residual epitaxial tensile strain $\varepsilon_\parallel^{epi}(y = 0.9, T_G)$ of the SiGe layer, present at the growth temperature, of the order of 10^{-4}, arising from its aforementioned incomplete plastic relaxation on the fully relaxed underlying Ge buffer region.[21] It is evident how the less mismatched $Si_{0.05}Ge_{0.95}$ VS, also shown in Fig. 1(d) for comparison, features a lower value of $\varepsilon_\parallel$.

The increase in the in-plane lattice strain value observed for a decreasing measurement temperature is fully accounted for by the following relationship, as discussed in Ref. 20:

$$\varepsilon_{\parallel}(y,T) = \varepsilon_{\parallel}^{therm}(y,T) + \varepsilon_{\parallel}^{epi}(y,T_G) \quad (1)$$

with

$$\varepsilon_{\parallel}^{therm}(y,T) = \int_{T}^{T_G} [\alpha_{Si_{1-y}Ge_y}(T') - \alpha_{Si}(T')]dT', \quad (2)$$

where T_G is the growth temperature and $\alpha_{Si_{1-y}Ge_y}$ and α_{Si} are the temperature dependent thermal expansion constants of the VS and Si wafer lattices whose functional dependence on T controls the negative slope observed in Fig. 1(d), respectively.

We now focus on the electronic band offsets at the $Si_{0.18}Ge_{0.82}$/Ge heterojunction, addressing first the role of the epitaxial strain. We show in Fig. 1(e) $\Delta E_{\Delta-L}$ and ΔE_{L-L} calculated at low T as a function of the y concentration in the relaxed VS. While the well depth ΔE_{L-L} is affected only weakly by the strain field, $\Delta E_{\Delta-L}$ significantly decreases upon increasing y, since the larger values of the tensile deformation shift downward the Δ_2 valleys in the barrier. Consequently, we expect that $\Delta E_{\Delta-L}$ also varies with T, since the thermal strain $\varepsilon_{\parallel}$(T) is itself temperature-dependent. To shed light on this point, in Fig. 1(f) we show $\Delta E_{\Delta-L}$ as a function of T, calculated for $y = 0.9$, both neglecting (dashed line) and including (continuous line) the thermal strain. In the first case, the energy difference is quite stable against temperature variations. Conversely, when thermal strain is taken into account, the room temperature (RT) value for $\Delta E_{\Delta-L}$ of 43 meV decreases down to about 32 meV at low T. This energy reduction significantly impacts the amount of carriers that can be transferred from the doped barrier into the well.

To observe and quantify this effect in realistic n-type Ge/SiGe multi-quantum-well systems, we have deposited on a $Si_{0.1}Ge_{0.9}$ VS a strain compensated structure made of 25 identical PQWs having well width $W = 61$ nm (sample S1). Its flatband potential profile associated with the L and Δ_2 edges and the related wavefunctions, calculated at 10 K, neglecting and considering the thermal strain, are shown in panels (a) and (b) of Fig. 2, respectively. The thermal strain has also been considered for RT calculations, reported in Fig. 2(c). In line with the above considerations, the lowest $\Delta E_{\Delta-L}$ value is obtained at low T, taking into account the thermal strain. Notice also that the amount of the energy effectively available to trigger the transfer doping may be further reduced by not equal confinement energies of Δ_2 and L subbands, related to different barrier and well layer thicknesses and confinement masses ($m_{\Delta_2} \simeq 0.9\, m_0$ and $m_L = 0.13\, m_0$).

Our simulations indicate that the PQWs host several confined states, with a constant energy separation $\hbar\omega_0 = 12$ meV (2.9 THz). The central 8 nm of the barrier layers have been doped with a donor concentration N_P of 8×10^{17} cm^{-3}, corresponding to a 2D carrier density per period of $n_{2D}^{tot} = 6.4 \times 10^{11}$ cm^{-2} to activate the ISBTs. The resulting electronic structures, obtained through the self-consistent solution of the Poisson equation and the multi-valley Schrödinger equation, are shown in panels (d) ($T = 10$ K, neglecting the thermal strain), (e) ($T = 10$ K, including thermal strain), and (f) ($T = 300$ K, including thermal strain) of Fig. 2. Note that, although the energy level spacing decreases for the Hartree contribution to the effective potential, the ISBT energy is still expected at the flatband value $\hbar\omega_0$, according to Kohn's theorem.[22] The role of the thermal strain in affecting the self-consistent potential profile is evident: the reduction of $\Delta E_{\Delta-L}$ predicted at low T when the effect of $\varepsilon_{\parallel}^{therm}$ is taken into account limits the amount of transferred charge, resulting in a weaker Hartree potential and a consequently deeper well.

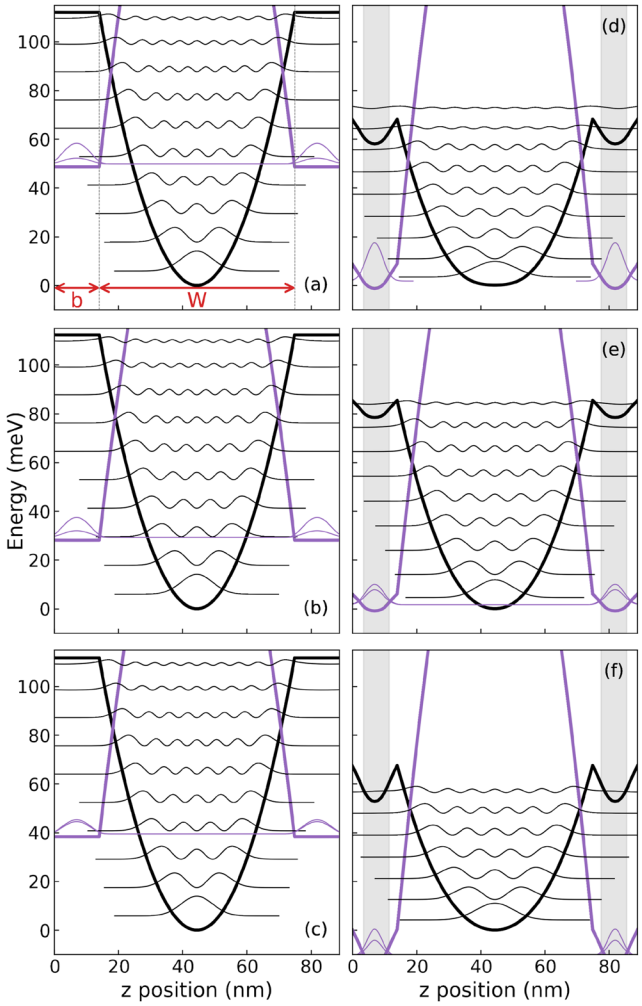

FIG. 2. Conduction band edge profiles at L (black line) and Δ_2 (purple line) along the growth direction z of sample S1. The well width W and barrier thickness b are 61 and 15 nm, respectively. The square modulus of the wavefunctions, plotted at the energy level of the corresponding quantized state, is also shown. Panels (a) and (b) show the flatband profiles calculated at 10 K, neglecting and including the thermal strain, respectively; and panel (c) shows the flatband profiles calculated at 300 K considering the thermal strain. Panels (d)–(f) are the same as panels (a)–(c) for the same structure doped in the central 8 nm of the barriers (gray region) with $N_P = 8 \times 10^{17}$ cm^{-3}.

The 2D carrier density in the L subbands calculated as a function of T, both including (red curve) and neglecting (blue curve) the thermal strain, is shown in Fig. 3(a). At RT, we obtain comparable values around $n_{2D}^{L} = 3.5 \times 10^{11}$ cm^{-2}, corresponding to a transfer

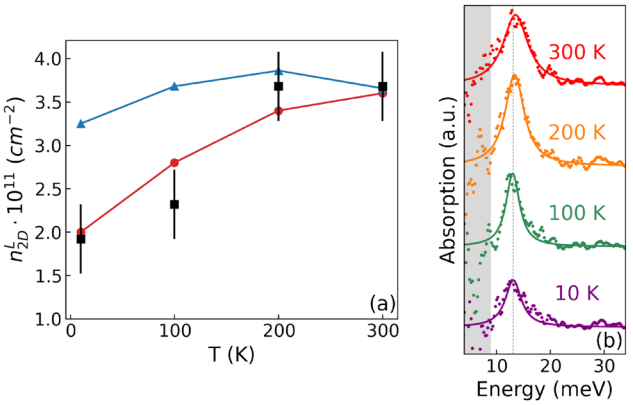

FIG. 3. (a) Calculated n_{2D}^L for sample S1 as a function of temperature, neglecting (blue curve) and taking into account (red curve) the thermal strain. Black symbols are the experimental values of n_{2D}^L obtained from the ISBT absorption spectra shown in panel (b).

efficiency $\eta = \frac{n_{2D}(L)}{n_{2D}^{tot}} = 50\%$. Lowering T, this ratio remains stable only if the $\varepsilon_{\parallel}^{therm}$ contribution to the strain field is neglected. Conversely, including this term, the transfer efficiency decreases to 30% at 10 K.

To validate these predictions, we have acquired by FTIR spectroscopy the dichroic transmission spectrum of the sample at different temperatures to isolate the ISBT contribution to the absorption spectrum and estimate the transferred charge density n_{2D}^L.[12] The ISBT absorption spectra reported in Fig. 3(b) feature a single peak at 12.8 meV (3.1 THz), in good agreement with the subband spacing estimated in the flatband condition $\hbar\omega_0$. Moreover, this peak energy remains extremely stable in the 10–300 K range, further confirming the achievement of a parabolic confinement potential in our compositionally graded PQWs. From the spectral weight of the 2D absorbance, we have estimated the sheet carrier density in the well, following the procedure reported in Ref. 12. The obtained experimental n_{2D}^L densities at different temperatures, reported in Fig. 3(a) as black squares, follow the monotonic behavior predicted by the model with the inclusion of $\varepsilon_{\parallel}^{therm}$, while they seem to be incompatible with the almost dispersionless blue curve. Remarkably, the observed reduction between RT and low T of n_{2D}^L values by a factor of 1.7 is also in agreement with the n_{2D}^L lowering estimated from the temperature dependence of the Rabi energy, measured in the ultrastrong-coupling regime in Ref. 5.

These findings highlight the critical role of thermal strain in controlling the transfer doping mechanism in n-type Ge/SiGe quantum structures and validate the predictability of the adopted theoretical model. Using this theoretical framework, we numerically investigated the transfer doping efficiency in PQWs having different widths W, i.e., designed to operate at different transition frequencies, and different dopings n_{2D}^{tot} in the [1–15] × 10^{11} cm^{-2} range. Our goal is to identify the configuration that maximizes carrier density in the well and/or transfer efficiency.

First, we performed simulations varying the PQW well width, keeping constant both the barrier thickness (15 nm) and the doping concentration (n_{2D}^{tot} = 1.5 × 10^{12} cm^{-2}). To preserve the strain compensation condition, the Ge concentration y in the VS was fine-tuned within the range [0.89–0.916]. The relative amount of transferred charge η as a function of T is shown in Fig. 4(a) for PQWs having ISBT at 3, 6, and 8 THz, corresponding to a well width of 58, 28, and 22 nm, respectively. We obtain a decrease in n_{2D}^L at low T for all the curves shown in Fig. 4(a).

Somewhat counterintuitively, the highest transfer efficiencies are achieved with the 8 THz PQWs, despite the higher confinement energy of the L subbands, which tends to lower $\Delta E_{\Delta-L}$ (note that the Δ_2 subbands are always found very close in energy to the Δ_2 band edge because of their large confinement mass). To understand this

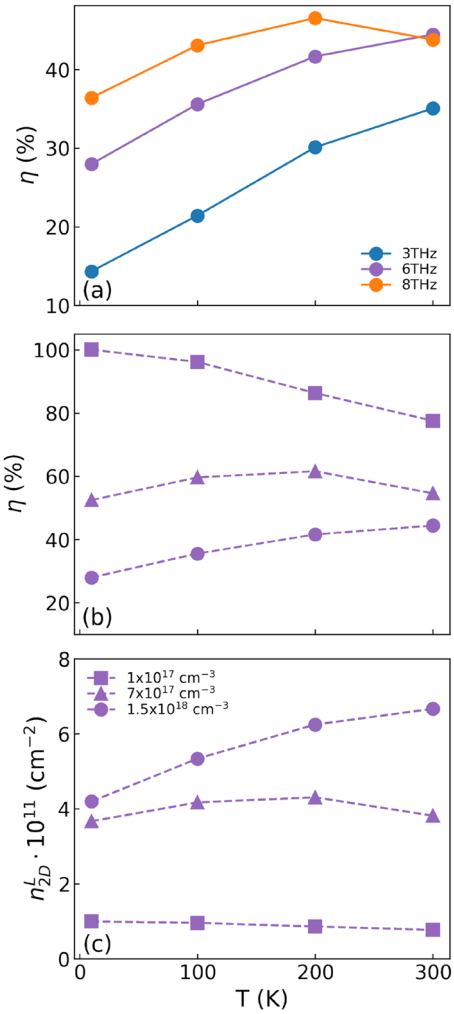

FIG. 4. (a) Calculated transfer efficiency η as a function of the temperature of PQWs having ISBT energy 3 (blue curve), 6 (purple curve), and 8 (orange curve) THz for n_{2D}^{tot} 1.5x10^{12} cm^{-2}. (b) Calculated transfer efficiency η and (c) transferred charge in the well n_{2D}^L as a function of temperature in 6 THz PQWs, for donor concentrations N_d = 1 × 10^{17} cm^{-3}, 7 × 10^{17} cm^{-3}, 1.5 × 10^{17} cm^{-3}, corresponding to sheet densities n_{2D}^{tot} = 1 × 10^{11} cm^{-2}) (squares), 7 × 10^{11} cm^{-2} (triangles), and 1.5 × 10^{12} cm^{-2} (circles), respectively.

effect, we observe that the transfer doping mechanism generates an electric field $\mathscr{E}$ in a region of width Δz between the center of the quantum well, where the electrons populate the L subbands, and the ionized donor region. This electric field is roughly equal to $\frac{n_{2D}^L}{\varepsilon}$ and produces a Hartree potential difference of about $\Delta V = \mathscr{E} \cdot \Delta z$, which reduces the energy separation of Δ_2 levels and L subbands. ΔV, for a fixed transferred charge, increases with Δz. Therefore, since the carrier flow toward the well stops when the energy of the lowest L subband states approaches the Δ_2 level in the barrier, lower values of Δz, featured just by thinner PQWs, allow larger amounts of n_{2D}^L. In the explored parameter range, upon decreasing the PQW width, this effect overcomes the adverse action related to higher confinement energies, thus resulting in larger n_{2D}^L densities.[23]

To investigate the charge transfer mechanism as a function of the doping density at different temperatures, we focus on the 6 THz PQW structure and plot the transfer efficiency η and the transferred charge density n_{2D}^L as a function of T, calculated for $n_{2D}^{tot} = 1 \times 10^{11}$, 7×10^{11}, and 1.5×10^{12} cm^{-2} [Figs. 4(b) and 4(c)].

We observe that for $n_{2D}^{tot} = 1 \times 10^{11}$ cm^{-2} and low T, the charge is fully transferred in the well due to the modest value of the Hartree potential difference ΔV. In this doping regime, the increase in $\Delta E_{\Delta-L}$ at higher temperatures caused by a decrease in $\varepsilon_{\parallel}^{therm}$ plays a minor role since the observed trend is dominated by the thermal excitation of carriers in the Δ_2 subbands, which controls the monotonic decrease in the transfer efficiency.

In the highest doping condition, we observe an opposite behavior since the transfer process is not complete at low T, η being of the order of 30% only. In fact, despite the reduced transfer efficiency, n_{2D}^L is large enough to equalize the energy of the lowest L subband states and the Δ_2 level in the barrier through the action of ΔV, stopping the transfer. In this condition, the increase in $\Delta E_{\Delta-L}$ at higher temperatures related to the lower $\varepsilon_{\parallel}^{therm}$ values enhances the amount of transferable carriers. The carrier transfer is also favored by the thermally induced population of excited L subbands. At the intermediate doping $n_{2D}^{tot} = 7 \times 10^{11}$ cm^{-2}, the carrier transfer is incomplete at low T with $\eta \simeq 50\%$, has a maximum at ~200 K, and then decreases at higher temperatures when the thermal excitation of Δ_2 levels becomes the dominant effect. In summary, from Figs. 4(b) and 4(c), we conclude that the optimal transfer efficiency is present at low T for 1×10^{11} cm^{-2}, while the largest absolute value of n_{2D}^L is obtained, in the investigated doping range, at RT for the highest doping density of 1.5×10^{12} cm^{-2}.

To further increase the transferred charge density in heavily doped samples, one can act on the tensile strain in the barrier, which can be reduced by depositing the PQW stack on a VS with a Ge content closer to the barrier. In this case, the strain-compensation condition is not satisfied, and the total thickness of the multilayered structure must not exceed the critical value for plastic relaxation.[8] To test this approach, we deposited two samples, S2 and S3, with the same multilayer structure, consisting of 15 modules of the 6 THz PQWs with doping $n_{2D}^{tot} = 1.5 \times 10^{12}$ cm^{-2} but deposited on VS substrates with different Ge compositions, i.e., $y = 0.89$ for the strain-compensated sample S2 and $y = 0.85$ for the not strain-compensated S3.

The analysis of XRD measurements, whose results are reported in the table included in Fig. 5, confirms the reproducibility of the

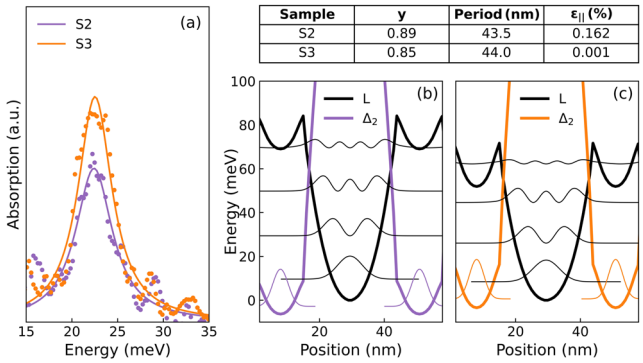

Sample	y	Period (nm)	$\varepsilon_{\parallel}$ (%)
S2	0.89	43.5	0.162
S3	0.85	44.0	0.001

FIG. 5. (a) ISBT absorption spectra of samples S2 (purple symbols) and S3 (orange symbols). (b) and (c) Band edge profiles and square modulus of the wavefunctions calculated for samples S2 and S3, respectively. In the table, the Ge content y in the VS, the period of the MPQW stack, and the average in-plane strain in the PQW stack, as determined from XRD data at 300 K, are reported.

nominally identical compositional profile in the PQW stacks of the two samples and the different strain fields, in agreement with the design values (see also the supplementary material). ISBT absorption spectra of the two samples are reported in Fig. 5(a). Both spectra consist of a single peak centered at 23 meV (5.5 THz), but the spectral weight of sample S3 is greater by a factor of 1.3, indicating that the transferred charge density in sample S3 is 30% higher with respect to the strain compensated one. This result is in line with the self-consistent band structures at 100 K reported in panels (b) and (c) for samples S2 and S3, respectively. The reduced tensile strain in the barrier featured by sample S3 has enabled a higher n_{2D}^L density, as testified also by the larger shrinking of the QW depth induced by the Hartree potential. Remarkably, we numerically find an increase in the transfer efficiency from 35% to 50%, perfectly matching the ratio of 1.3 for the carrier density estimated by comparing the two spectral weights of Fig. 5(a).

In conclusion, we have combined XRD measurements and FTIR ISBT spectroscopy performed on n-type Ge/SiGe PQWs with their numerical modeling to shed light on the different physical effects controlling the charge transfer process in modulation-doped, Ge-rich Ge/SiGe quantum heterostructures. Our analysis shows how the efficiency of the charge transfer is critically affected by the epitaxial and thermal strain through their impact on the energy separation between the conduction band minima in the well and in the barrier material. In addition, we have numerically studied the transfer efficiency as a function of the donor concentration in the barrier and the well width in order to optimize the design to achieve either the highest carrier density in the well or the maximum transfer efficiency. Indeed, an efficiency of 100% is predicted at low T and for a carrier density of about 1×10^{11} cm^{-2}, while the largest absolute value of n_{2D}^L is obtained at RT for the highest investigated doping density of 1.5×10^{12} cm^{-2}, with an efficiency of about 50%. We believe that the improved degree of control over the transfer doping process, achieved in this work, represents an important step forward toward the realization of novel quantum

optoelectronic devices based on this CMOS-compatible material system.

In the supplementary material, we report and discuss the 224 reciprocal space maps from the strain-compensated S2 sample and the strain unbalanced S3 sample.

M.D.S. and L.D.G. acknowledge the support of PNRR MUR project PE0000023-NQSTI Spoke 4 CUP B53C22004170006 (Bando a cascata domanda n. 0002/24 "THE UPSIDE") M.V., L.D.G., D.M., and M.D.S. acknowledge the support from the Italian MUR grant PRIN 2022 PNRR Integrable Thz Si-based Quantum Cascade Operation, Mission 4 Component 2, CUP I53D23006680001, funded by the European Union—NextGenerationEU. Part of this work has been carried out within the Joint Lab "Intelligent Electro-Optical Sensing," established between IHP and the University of Rome Tre.

AUTHOR DECLARATIONS

Conflict of Interest

The authors have no conflicts to disclose.

Author Contributions

E. Campagna: Data curation (equal); Investigation (equal); Visualization (equal); Writing – original draft (equal). **E. Talamas Simola**: Conceptualization (equal); Data curation (equal); Investigation (equal); Supervision (equal); Writing – review & editing (equal). **L. Di Gaspare**: Investigation (equal); Methodology (equal); Supervision (equal); Writing – review & editing (equal). **D. Marian**: Formal analysis (equal); Writing – review & editing (equal). **M. H. Zoellner**: Data curation (equal); Investigation (equal); Validation (equal). **F. Berkmann**: Data curation (equal); Investigation (equal). **L. Baldassarre**: Data curation (equal); Investigation (equal). **M. Ortolani**: Data curation (equal); Investigation (equal). **G. Capellini**: Formal analysis (equal); Investigation (equal); Resources (equal); Supervision (equal); Writing – review & editing (equal). **M. Virgilio**: Conceptualization (equal); Funding acquisition (equal); Investigation (equal); Methodology (equal); Software (equal); Supervision (lead); Writing – original draft (lead); Writing – review & editing (equal). **M. De Seta**: Conceptualization (lead); Funding acquisition (equal); Investigation (equal); Methodology (equal); Resources (lead); Supervision (lead); Writing – original draft (lead); Writing – review & editing (equal).

DATA AVAILABILITY

The data that support the findings of this study are available from the corresponding author upon reasonable request.

REFERENCES

[1]I. A. Fischer, M. Brehm, M. De Seta, G. Isella, D. J. Paul, M. Virgilio, and G. Capellini, "On-chip infrared photonics with Si–Ge-heterostructures: What is next?," APL Photonics **7**, 050901 (2022).
[2]D. J. Paul, "The progress towards terahertz quantum cascade lasers on silicon substrates," Laser Photonics Rev. **4**, 610–632 (2010).
[3]T. Grange, D. Stark, G. Scalari, J. Faist, L. Persichetti, L. Di Gaspare, M. De Seta, M. Ortolani, D. J. Paul, G. Capellini, S. Birner, and M. Virgilio, "Room temperature operation of *n*-type Ge/SiGe terahertz quantum cascade lasers predicted by non-equilibrium Green's functions," Appl. Phys. Lett. **114**, 111102 (2019).
[4]D. Stark, M. Mirza, L. Persichetti, M. Montanari, S. Markmann, M. Beck, T. Grange, S. Birner, M. Virgilio, C. Ciano, M. Ortolani, C. Corley, G. Capellini, L. Di Gaspare, M. De Seta, D. J. Paul, J. Faist, and G. Scalari, "THz intersubband electroluminescence from n-type Ge/SiGe quantum cascade structures," Appl. Phys. Lett. **118**, 101101 (2021).
[5]F. Berkmann, T. Venanzi, L. Baldassarre, E. Campagna, E. Talamas Simola, L. Di Gaspare, C. Corley-Wiciak, G. Capellini, G. Nicotra, G. Sfuncia, A. Notargiacomo, E. Giovine, S. Cibella, M. Virgilio, G. Scalari, M. De Seta, and M. Ortolani, "Ultrastrong coupling of $Si_{1-x}Ge_x$ parabolic quantum wells to terahertz microcavities," ACS Photonics **11**, 2776 (2024).
[6]T. Grange, S. Mukherjee, G. Capellini, M. Montanari, L. Persichetti, L. Di Gaspare, S. Birner, A. Attiaoui, O. Moutanabbir, M. Virgilio, and M. De Seta, "Atomic-scale insights into semiconductor heterostructures: From experimental three-dimensional analysis of the interface to a generalized theory of interfacial roughness scattering," Phys. Rev. Appl. **13**, 044062 (2020).
[7]M. Montanari, C. Ciano, L. Persichetti, C. Corley, L. Baldassarre, M. Ortolani, L. Di Gaspare, G. Capellini, D. Stark, G. Scalari, M. Virgilio, and M. De Seta, "THz intersubband absorption in n-type $Si_{1-x}Ge_x$ parabolic quantum wells," Appl. Phys. Lett. **118**, 163106 (2021).
[8]E. Talamas Simola, M. Montanari, C. Corley-Wiciak, L. Di Gaspare, L. Persichetti, M. H. Zöllner, M. A. Schubert, T. Venanzi, M. C. Trouche, M. Ortolani, F. Mattioli, G. Sfuncia, G. Nicotra, G. Capellini, M. Virgilio, and M. De Seta, "Subnanometer control of the heteroepitaxial growth of multimicrometer-thick Ge/Si–Ge quantum cascade structures," Phys. Rev. Appl. **19**, 014011 (2023).
[9]W. Cao, H. Bu, M. Vinet, M. Cao, S. Takagi, S. Hwang, T. Ghani, and K. Banerjee, "The future transistors," Nature **620**, 501–515 (2023).
[10]F. T. Armand Pilon, Y.-M. Niquet, J. Chretien, N. Pauc, V. Reboud, V. Calvo, J. Widiez, J. M. Hartmann, A. Chelnokov, J. Faist, and H. Sigg, "Investigation of lasing in highly strained germanium at the crossover to direct band gap," Phys. Rev. Res. **4**, 033050 (2022).
[11]K. Driscoll and R. Paiella, "Design of *n*-type silicon-based quantum cascade lasers for terahertz light emission," J. Appl. Phys. **102**, 093103 (2007).
[12]Y. Busby, M. De Seta, G. Capellini, F. Evangelisti, M. Ortolani, M. Virgilio, G. Grosso, G. Pizzi, P. Calvani, S. Lupi *et al.*, "Near- and far-infrared absorption and electronic structure of Ge–SiGe multiple quantum wells," Phys. Rev. B **82**, 205317 (2010).
[13]K. Isensee, N. Kröger-Lui, and W. Petrich, "Biomedical applications of mid-infrared quantum cascade lasers—A review," Analyst **143**, 5888–5911 (2018).
[14]J. Ulrich, R. Zobl, K. Unterrainer, G. Strasser, E. Gornik, K. D. Maranowski, and A. C. Gossard, "Temperature dependence of far-infrared electroluminescence in parabolic quantum wells," Appl. Phys. Lett. **74**, 3158–3160 (1999).
[15]M. Geiser, F. Castellano, G. Scalari, M. Beck, L. Nevou, and J. Faist, "Ultrastrong coupling regime and plasmon polaritons in parabolic semiconductor quantum wells," Phys. Rev. Lett. **108**, 106402 (2012).
[16]C. Deimert, P. Goulain, J.-M. Manceau, W. Pasek, T. Yoon, A. Bousseksou, N. Y. Kim, R. Colombelli, and Z. R. Wasilewski, "Realization of harmonic oscillator arrays with graded semiconductor quantum wells," Phys. Rev. Lett. **125**, 097403 (2020).
[17]L. Brey, N. F. Johnson, and B. I. Halperin, "Optical and magneto-optical absorption in parabolic quantum wells," Phys. Rev. B **40**, 10647 (1989).
[18]M. Geiser, G. Scalari, F. Castellano, M. Beck, and J. Faist, "Room temperature terahertz polariton emitter applied physics letters," Appl. Phys. Lett. **101**, 141118 (2012).
[19]E. Campagna, E. Talamas Simola, T. Venanzi, F. Berkmann, C. Corley-Wiciak, G. Nicotra, L. Baldassarre, G. Capellini, L. Di Gaspare, M. Virgilio, M. Ortolani, and M. De Seta, "High-quality CMOS compatible n-type SiGe parabolic quantum wells for intersubband photonics at 2.5–5 THz," Nanophotonics **13**, 1793–1802 (2024).

[20]G. Capellini, M. De Seta, P. Zaumseil, G. Kozlowski, and T. Schroeder, "High temperature x ray diffraction measurements on Ge/Si(001) heterostructures: A study on the residual tensile strain," J. Appl. Phys. **111**, 073518 (2012).
[21]O. Skibitzki, M. H. Zoellner, F. Rovaris, M. A. Schubert, Y. Yamamoto, L. Persichetti, L. Di Gaspare, M. De Seta, R. Gatti, F. Montalenti, and G. Capellini, "Reduction of threading dislocation density beyond the saturation limit by optimized reverse grading," Phys. Rev. Mater. **4**, 103403 (2020).
[22]W. Kohn, "Cyclotron resonance and de Haas-van Alphen oscillations of an interacting electron gas," Phys. Rev. **123**, 1242 (1961).
[23]The tiny variations in the strain field related to the tuning of y in the VS have a negligible impact on the transferred charge density.